

Hourly measurement of cosmic ray anisotropy by LHAASO WCDA at ~ 1 TeV: Effects of an interplanetary flux rope during 2021 November

Kritsanon Koennonkok,^{a,*} David Ruffolo,^a Warit Mitthumsiri^a and Wei Liu^{b,c} on behalf of the LHAASO Collaboration

^aDepartment of Physics, Faculty of Science, Mahidol University, Bangkok 10400, Thailand

^bKey Laboratory of Particle Astrophysics & Experimental Physics Division & Computing Center, Institute of High Energy Physics, Chinese Academy of Sciences, 100049 Beijing, China

^cTianfu Cosmic Ray Research Center, 610000 Chengdu, Sichuan, China

E-mail: kritsanon.k@kkumail.com, david.ruf@mahidol.ac.th

Interplanetary coronal mass ejections (ICMEs) are known to affect the intensity and anisotropy of Galactic cosmic rays of energies up to ~ 100 GeV, but effects at higher energies have rarely been reported. Here we analyze data from the Large High Altitude Air Shower Observatory (LHAASO), and in particular its Water Cherenkov Detector Array (WCDA), which has been in full operation since March 2021. WCDA is sensitive to primary cosmic rays above about 100 GeV with a wide field of view (FOV), from which we select events within 45 degrees of the zenith. We normalize cosmic ray skymaps relative to a monthly average. Then for each hour of data, we express the cosmic ray anisotropy as the gradient of the excess cosmic ray rate over the FOV. For the ICME passage of 2021 Nov 4-5, a strong anisotropy was recently reported in data from muon detectors and neutron monitors. We present evidence for an enhanced anisotropy in LHAASO-WCDA data during that time period, for primary cosmic ray energy ranges both below and above 1 TeV.

38th International Cosmic Ray Conference (ICRC2023)
26 July - 3 August, 2023
Nagoya, Japan



*Speaker

1. Introduction

The flux and anisotropy of Galactic cosmic ray (CR) ions are believed to be constant over time scales of decades before they encounter our heliosphere. Within our heliosphere, different types of time variations due to solar and heliospheric phenomena have been documented for GeV-range ions, including effects of the ~ 11 -year solar activity (sunspot) cycle [1], ~ 22 -year solar magnetic cycle [2], ~ 27 -day solar rotation [3], and transient effects of solar storms and solar wind variations such as Forbush decreases [4]. However, the maximum energy of such effects remains unclear. Because solar-heliospheric effects become weaker with increasing particle energy, with variations of at most several percent above ~ 20 GeV [5], their measurement at much higher energy requires the statistics of large ground-based detectors.

Previous work has reported solar cycle effects on the CR anisotropy from the Matsushiro underground muon detector, sensitive to a median CR rigidity of 0.6 TeV [6], while no long-term variation was found in the solar diurnal anisotropy measured during 2000-2009 at ~ 4 TeV by the Tibet Air Shower Array [7]. Time variability has been observed in the Sun shadow of TeV-range ions, including dependence on the sign of the interplanetary magnetic field [8], variation with the solar activity cycle [9], and the superposed effect of solar storms [10].

In the present work, we examine a different effect: transient variation of large-scale CR anisotropy due to a solar storm. We have developed techniques to analyze the hourly anisotropy from the Water Cherenkov Detector Array (WCDA) of the Large High-Altitude Air Shower Observatory (LHAASO). We present what may be the first observation of transient variation in large-scale anisotropy at energies below and above 1 TeV, associated with the passage of a shock and interplanetary coronal mass ejection (ICME) on 2021 November 4.

2. LHAASO data

LHAASO is a hybrid detector system located at Mt. Haizi, Sichuan, China, at an altitude of 4,410 meters above sea level. One component of LHAASO is WCDA, consisting of 3 water ponds with total area of 78,000 m². This large detection area (with $\approx 97\%$ duty cycle) and a wide FOV enable the precise measurement of large-scale CR anisotropy with an hourly cadence [11]. We use the Mk dataset, which will be described in detail elsewhere, comprising data since full operation commenced on 2021 March 5. The WCDA ponds are divided into 3,120 cells of 5 m \times 5 m, separated by black plastic curtains. The energy of the primary CR generating each shower is estimated using N_{hit} , the number of cells registering a significant signal, in coincidence with the shower according to the criteria of [12].

For this preliminary analysis, we use two N_{hit} ranges: 1) $30 \leq N_{hit} < 100$, which according to Monte Carlo simulations is sensitive to a wide primary CR energy range of ≈ 0.1 -100 TeV with a median energy near 1 TeV, and 2) $320 \leq N_{hit} < 2025$, which is exclusively above 1 TeV with a median energy near 10 TeV. Therefore, the lower range includes CRs both below and above 1 TeV, while the higher range only includes CRs above 1 TeV.

3. Methods

3.1 Hourly cosmic ray skymap

This analysis is limited to events with a zenith angle below 45° , to avoid strong fluctuations due to poorer statistics at higher zenith angle, and to avoid bias as the correspondence between primary energy and N_{hit} is quite different at large zenith angle. For each hour of data, we create a skymap of the number of shower events divided into sections according to 16 ranges of the azimuthal angle and 8 ranges of the zenith angle, regularly spaced in the zenith angle cosine so that each section corresponds to a similar solid angle (see Figure 1). For each month, we create a standard skymap for each hour of day (basically corresponding to different 24 look directions in the sky as Earth rotates), averaging for each hour of good data within that month; this results in 24 standard skymaps per month. Both hourly and standard skymaps are normalized by the average value along each zenith angle range in that day or month, respectively (to remove dependence of the count rate on zenith angle), and each hourly skymap is divided by the corresponding standard skymap.

The results from 2021 Apr to 2022 Nov are qualitatively consistent with a combination of the known large-scale sidereal anisotropy [e.g., 13] and the Compton-Getting anisotropy due to Earth's motion around the Sun [14]. The combination of these two patterns varies with Earth's position along its orbit, and indeed we find good consistency between standard skymaps for the same month in different years.

3.2 Cosmic ray gradient vector

We quantitatively characterize a normalized hourly skymap in terms of a CR gradient vector \mathbf{g} . For each skymap value R_i at zenith angle θ_i and azimuthal angle φ_i (counterclockwise from the East direction), we define $x_i = \sin \theta_i \cos \varphi_i$ and $y_i = \sin \theta_i \sin \varphi_i$. The linear least squares fitting of $R_i(x_i, y_i)$ by $1 + g_x x_i + g_y y_i$ results in gradient components

$$g_x = \frac{\sum_i x_i (R_i - 1)}{\sum_i x_i^2}, \quad g_y = \frac{\sum_i y_i (R_i - 1)}{\sum_i y_i^2}$$

in the eastward and northward directions, respectively. In the case of a dipole anisotropy directed perpendicular our zenith direction, the magnitude $g \equiv |\mathbf{g}|$ would equal the amplitude of dipole anisotropy. In further work, we plan to model the “background” gradient expected from the known (measured) sidereal diurnal anisotropy and the calculated Compton-Getting solar diurnal anisotropy, to verify that the quiet-time profile of \mathbf{g} can be explained by these effects. Following [15] we transform \mathbf{g} to geocentric solar ecliptic (GSE) coordinates, for comparison with other solar-heliospheric data (such as the sunward or interplanetary magnetic field direction) and to facilitate comparison with the transient anisotropy observed in lower-energy CR ions [16].

3.3 Comparison with anisotropy measured by neutron monitors and muon detectors

From an analysis of data from neutron monitors and muon detector worldwide, with a total of 90 asymptotic look directions, [16] analyzed a particularly strong transient anisotropy around the times of passage of an interplanetary shock and ICME on 2021 November 3-5. Most of the 21 neutron monitors were sensitive to a median CR rigidity close to 15 GV, while a typical median

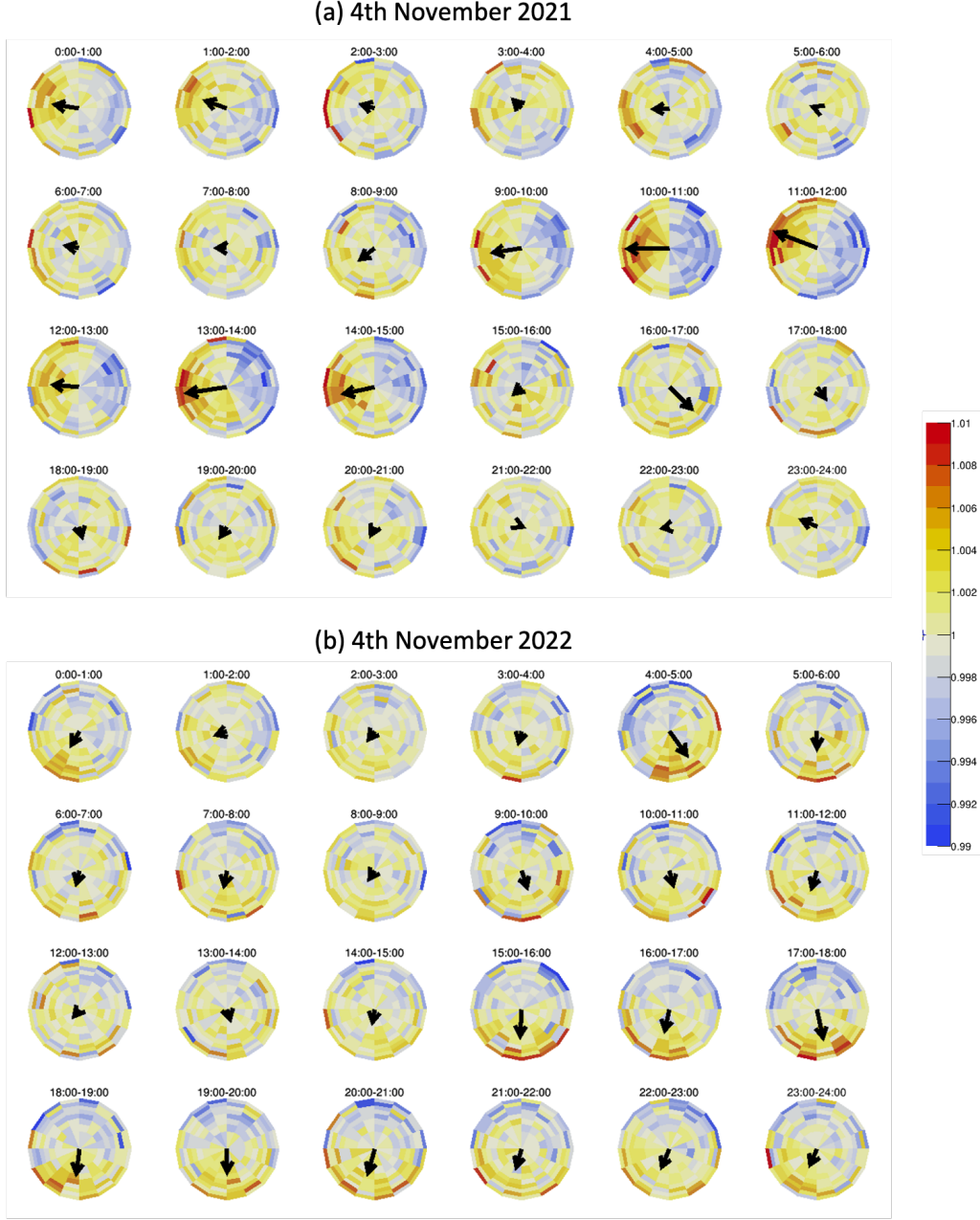


Figure 1: Preliminary hourly WCDA skymaps centered at the zenith direction, out to a zenith angle of 45° (outer circle), for $30 \leq N_{hit} < 100$ for each hour UT of (a) 2021 Nov 4, when an ICME arrived at Earth, and (b) 2022 Nov 4, as a quiet time for comparison. In each skymap, directions northward from the zenith are at the top and directions eastward of the zenith are at the right. The black arrow indicates the best-fit CR gradient vector, The length of the arrow is proportional to the gradient magnitude, pointing away from directions with a deficit (blue) and toward those with an enhancement (red). During quiet times (e.g., averaged over every day of a month), the gradient vector exhibits a systematic variation that repeats from year to year and is qualitatively consistent with a combination of known sidereal and Compton-Getting (solar) diurnal variations. Around the time of ICME arrival, midday on 2021 Nov 4, there was a marked enhancement in the anisotropy and the gradient magnitude.

rigidity for the 69 muon detector channels was 65 GV. In Figure 2(a) we display their fit results for the 1st- and 2nd-order anisotropy of 65 GV CR ions, and the time of arrival of the interplanetary shock and start and end times of passage of a magnetic flux rope (MFR). Motivated by this result, and the prospect of a direct comparison with results for lower-energy CRs, we searched for and found an enhanced CR anisotropy below and above 1 TeV in WCDA data during this time period.

4. Preliminary results

We examined hourly skymaps to search for evidence of extra, transient anisotropy, in addition to the usual pattern associated with known sidereal and Compton-Getting (solar) diurnal anisotropy. Figure 1(a) shows the hourly skymaps for 2021 Nov 4, when the MFR of the ICME arrived at Earth, while Figure 1(b) shows the hourly skymaps for 2022 Nov 4 as a quiet time for comparison. There was a marked enhancement in anisotropy in the FOV during 0900-1700 UT on 2021 Nov 4, around the time of MFR arrival (which was near 1200 UT).

Figures 2(b) and 2(c) show the gradient vector from our preliminary analysis of WCDA data for the two N_{hit} ranges. The gradient was strongly enhanced relative to quiet times. We were expecting that the transient anisotropy reported by [16] might extend only to energies of ~ 100 GeV (the muon detector channels analyzed in that work had a median rigidity response of at most 107 GV). As a reminder, the lower N_{hit} range used for Figure 2(b) is due to primary CR ions with a median energy of ~ 1 TeV and some response all the way from about 100 GeV to 100 TeV, so the enhanced anisotropy in this N_{hit} range could conceivably be attributed to effects at ~ 100 GeV. However, Figure 2(c) is for $320 \leq N_{hit} < 2025$, which according to Monte Carlo simulation should respond only to CR ions above 1 TeV, with a median response to ~ 10 TeV.

Figure 3 shows our preliminary cosmic ray gradient vector for each hour, for the two N_{hit} ranges, as an arrow starting from the zenith direction and pointing in the gradient direction as transformed to GSE coordinates, with a length proportional to the gradient magnitude. The black curve indicates the WCDA FOV in these coordinates.

One limitation of our technique is that it only measures the CR gradient over a FOV within 45° from LHAASO's zenith direction. Any true anisotropy pattern will have at least one local minimum and one local maximum, and if the zenith direction is near such an extreme point, the gradient should be suppressed. Thus while observation of a strong gradient is evidence of a strong anisotropy pattern, a weak gradient near the zenith direction does not necessarily imply that the overall anisotropy pattern is weak.

Note also that the gradient vectors plotted in Figures 1-3 include the gradient due to the quiet-time sidereal and solar diurnal anisotropy, as well as any transient anisotropy.

5. Summary

Thus our preliminary conclusion is that we have found transient large-scale anisotropy in association with an ICME on 2021 Nov 4, for energies both below and above 1 TeV. In further work, we intend to calculate and subtract the gradient due to the “background” anisotropy; only the additional transient anisotropy gradient should be associated with the ICME and compared with the direction of the interplanetary magnetic field.

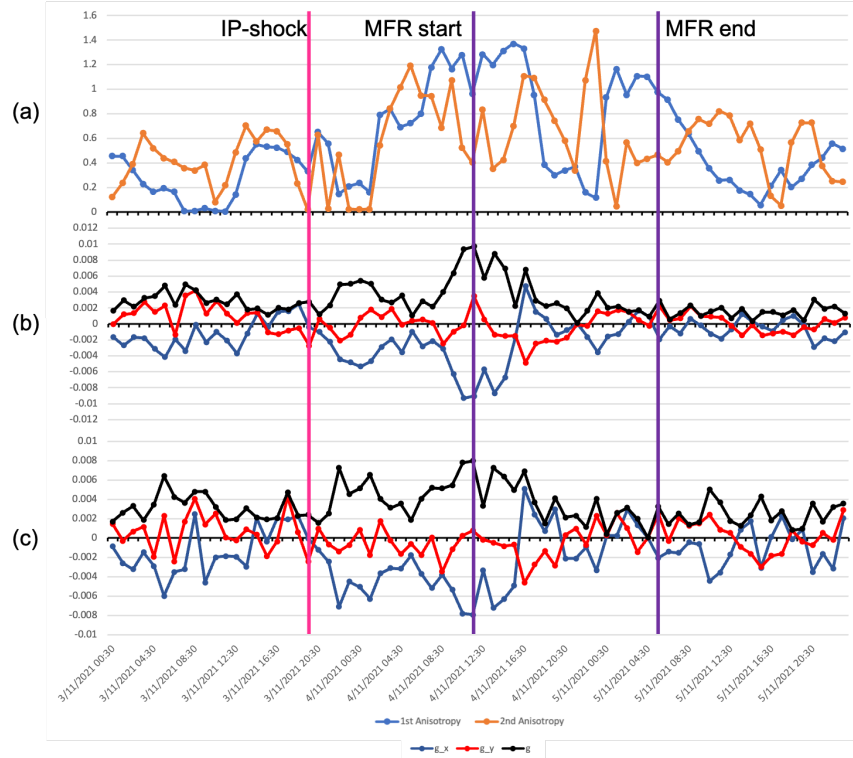


Figure 2: (a) Amplitudes of 1st- and 2nd-order anisotropy of 65 GV CR ions, in percent, as reported by [16]. Also plotted is the preliminary WCD gradient vector for (b) $30 \leq N_{hit} < 100$, for median CR energy ~ 1 TeV, and (c) $320 \leq N_{hit} < 2025$, for CRs of > 1 TeV, including the x-component (blue), y-component (red) and magnitude (black). Vertical pink line indicates time of interplanetary shock arrival. Two purple lines indicate time period of passage of the ICME’s magnetic flux rope (MFR). The time of enhanced CR anisotropy below and above 1 TeV in LHAASO’s field of view corresponds to the sheath region between the shock and MFR and the early portion of the MFR.

6. Acknowledgements

We extend our gratitude to all members of the LHAASO teams, especially those who work year-round at the LHAASO site, located over 4400 m above sea level. We are grateful to all sources of funding for LHAASO. In addition, K.K. is grateful to the Development and Promotion of Science and Technology Talents Project (DPST) for the funding and all support. Work in Thailand was supported by the National Science and Technology Development Agency (NSTDA) and the National Research Council of Thailand (NRCT) under the High-Potential Research Team Grant Program (N42A650868), and from the NSRF via the Program Management Unit for Human Resources & Institutional Development, Research and Innovation (B37G660015).

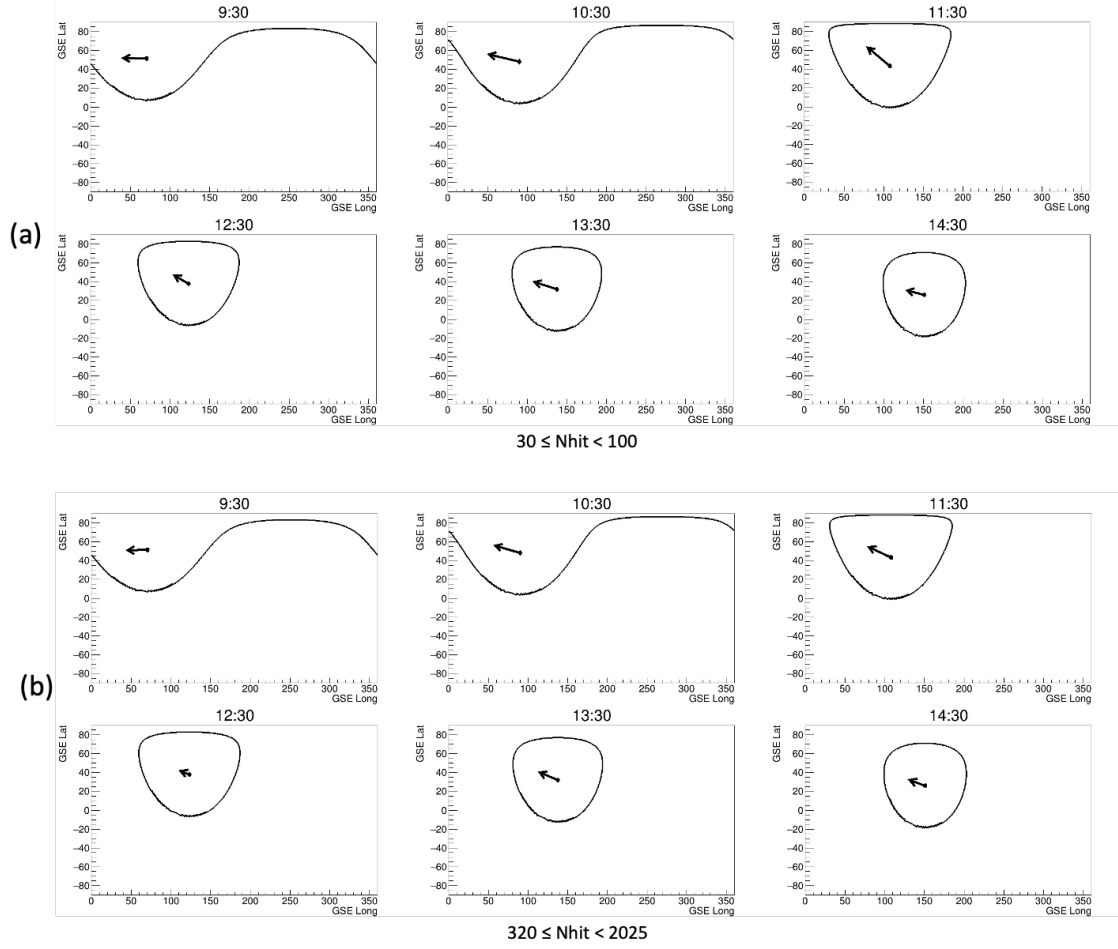


Figure 3: Black arrows indicate the magnitude and direction of the CR gradient from our preliminary analysis of WCDa measurements during hours centered at 0930 to 1430 UT on 2021 Nov 4 for (a) $30 \leq N_{hit} < 100$, with median CR energy ~ 1 TeV, and (b) $320 \leq N_{hit} < 2025$, for CRs of > 1 TeV. The arrow starts from a solid circle at the zenith direction, and the black curve indicates the edge of our FOV at an angular distance of 45° from the zenith.

References

- [1] S.E. Forbush, *World-Wide Cosmic-Ray Variations, 1937-1952*, *J. Geophys. Res.* **59** (1954) 525.
- [2] T. Thambyahpillai and H. Elliot, *World-wide changes in the phase of the cosmic-ray solar daily variation*, *Nature* **171** (1953) 918.
- [3] W.H. Fonger, *Cosmic Radiation Intensity-Time Variations and Their Origin. II. Energy Dependence of 27-Day Variations*, *Phys. Rev.* **91** (1953) 351.
- [4] S.E. Forbush, *On the Effects in Cosmic-Ray Intensity Observed During the Recent Magnetic Storm*, *Phys. Rev.* **51** (1937) 1108.

- [5] D. Ruffolo, *Time variations in Galactic cosmic rays as measured from Southeast Asia*, in *J. Phys.: Conf. Ser.*, vol. 1572, p. 012087, June, 2020, [DOI](#).
- [6] K. Munakata, Y. Mizoguchi, C. Kato, S. Yasue, S. Mori, M. Takita et al., *Solar Cycle Dependence of the Diurnal Anisotropy of 0.6 TeV Cosmic-ray Intensity Observed with the Matsushiro Underground Muon Detector*, *Astrophys. J.* **712** (2010) 1100 [[0911.1165](#)].
- [7] M. Amenomori, X.J. Bi, D. Chen, T.L. Chen, W.Y. Chen, S.W. Cui et al., *On the Solar Cycle Variation of the Solar Diurnal Anisotropy of Multi-TeV Cosmic-ray Intensity Observed with the Tibet Air Shower Array*, in *European Physical Journal Web of Conferences*, vol. 208 of *European Physical Journal Web of Conferences*, p. 08012, May, 2019, [DOI](#).
- [8] M. Amenomori, Z. Cao, L.K. Ding, Z.Y. Feng, K. Hibino, N. Hotta et al., *Direct Evidence of the Interplanetary Magnetic Field Effect on the Cosmic-Ray Shadow by the Sun*, *Astrophys. J. Lett.* **415** (1993) L147.
- [9] M. Amenomori, B.Z. Dai, L.K. Ding, Z.Y. Feng, K. Hibino, N. Hotta et al., *Shadowing of Cosmic Rays by the Sun near Maximum or at the Declining Phase of Solar Activity*, *Astrophys. J.* **464** (1996) 954.
- [10] M. Amenomori, X.J. Bi, D. Chen, T.L. Chen, W.Y. Chen, S.W. Cui et al., *Influence of Earth-directed Coronal Mass Ejections on the Sun's Shadow Observed by the Tibet-III Air Shower Array*, *Astrophys. J.* **860** (2018) 13 [[1806.03387](#)].
- [11] X.-H. Ma, Y.-J. Bi, Z. Cao, M.-J. Chen, S.-Z. Chen, Y.-D. Cheng et al., *Chapter 1 LHAASO Instruments and Detector technology*, *Chinese Physics C* **46** (2022) 030001.
- [12] F. Aharonian, Q. An, Axikegu, L.X. Bai, Y.X. Bai, Y.W. Bao et al., *Performance of LHAASO-WCDA and observation of the Crab Nebula as a standard candle*, *Chinese Physics C* **45** (2021) 085002.
- [13] B. Bartoli, P. Bernardini, X.J. Bi, Z. Cao, S. Catalanotti, S.Z. Chen et al., *Galactic Cosmic-Ray Anisotropy in the Northern Hemisphere from the ARGO-YBJ Experiment during 2008-2012*, *Astrophys. J.* **861** (2018) 93 [[1805.08980](#)].
- [14] S. Yasue, S. Mori, K. Munakata, A.A. Darwish and A.A. Bishara, *Observation of earth's orbital motion using cosmic-ray Compton-Getting effect at Matsushiro underground station*, *J. Geomag. Geoelec.* **43** (1991) 771.
- [15] M.A. Hapgood, *Space physics coordinate transformations: A user guide*, *Planet. Space Sci.* **40** (1992) 711.
- [16] K. Munakata, M. Kozai, C. Kato, Y. Hayashi, R. Kataoka, A. Kadokura et al., *Large-amplitude Bidirectional Anisotropy of Cosmic-Ray Intensity Observed with Worldwide Networks of Ground-based Neutron Monitors and Muon Detectors in 2021 November*, *Astrophys. J.* **938** (2022) 30 [[2209.05743](#)].